*Desalination and Water Treatment*
www.deswater.com
doi: 10.5004/dwt.2023.30136

315 (2023) 287–303
December

# Investigation and optimization of design parameters for the thermal performance of a flat-plate solar air heater with sensible heat storage medium

Mariyappan Selvaraj[a,*], Palaniswamy Sadagopan[b], Selvaraj Vijayan[c]

[a]*Department of Mechanical Engineering, Gnanamani College of Technology, Namakkal-637 018, Tamil Nadu, India, Tel.: +91 9442360699; email: npselvarajj@gmail.com*
[b]*Professor Retired and Industrial Consultant, Coimbatore, Tamil Nadu, India, email: sadagopan.p@gmail.com*
[c]*Department of Mechanical Engineering, Coimbatore Institute of Engineering and Technology, Coimbatore-641 109, India, email: vijayandakshinya@gmail.com*

Received 7 June 2023; Accepted 6 November 2023

**ABSTRACT**

The thermal performance of a flat-plate solar air heater with airflow through a specially designed twin copper fin plate was investigated experimentally using a solar thermal simulator fitted with a halogen lamp. The effects of the parameters, *viz.*, airflow, glass cover thickness, absorber plate materials, sensible heat storage materials, and insulating materials, on the thermal performance of the dryer were studied using Taguchi's design of experiments with an L27 orthogonal array and optimized using analysis of variance. In this research study, it was found that an average temperature gain of 17.579°C is achieved for the combination of significant factors, *viz.*, coconut fibre insulation, a 4 mm thick glass cover, a copper absorber plate, aluminium scrap storage material, and an air mass flow rate of 0.02 kg/s.

*Keywords:* Flat-plate solar air heater; Thermal performance; Taguchi method; Optimization; Analysis of variance; Temperature gain; Sensible heat storage medium

## 1. Introduction

Solar drying is one of the techniques used to remove moisture from agricultural products. In most rural areas, open-sun drying is adopted, as it is very easy to handle and there is no energy bill involved. However, dust and other issues from birds, animals, and human intervention affect the processing of open sun dehydrating hygienically. The quality of drying of agricultural products is influenced by the air temperature, air velocity, humidity of the atmosphere, surface area, and size of the crop. In the case of small-scale processing, the drying is usually carried out by means of electrical or mechanical dryers. They mostly use high-grade fossil or energy fuels, which makes the drying process extra expensive. The best substitute for mechanical dryers is solar drying; solar energy is hygienic and freely available. Over the years, many solar dryers have been established with various performance improvement techniques, such as the integration of enhanced solar collectors, energy storage materials, etc., and their performances have been studied for drying various agricultural food products. The broad literature survey of indirect solar dehydrating revealed that the addition of sensible heat storage resources enhances the performance of a dryer. Sensible heat storage resources are simple and easy to integrate into the airflow path for attaining consistent hot air for the drying process.

In order to study the effects of various factors on the performance of solar dryers, a steady heat radiation source is required. Direct solar radiation power cannot be used since it varies due to the formation of clouds, humidity, dust level, and incident angle on the collector; hence, the use of direct solar radiation is not considered in this study. In order to have a steady heat source, a halogen lamp set was fabricated, and the experiments were conducted in a room. However,

* Corresponding author.

the effect of voltage variations in the experimental setup was not considered, which influences the power output of the halogen lamp as it is random.

Numerous researchers have modeled the flat-plate solar air dryer to dry fruits, vegetables, roots, herbs, seeds, meat, etc. Ezeanya et al. [1] discussed the drying kinetics of cassava noodles. They reported that the maximum drying rate of 39.2%/h was obtained during the experiment. For drying mango pieces, Eustache et al. [2] prepared rock as a sensible heat storage medium in a mixed method using a natural convection solar dryer with two systems: the first method is the flat-plate solar collector with an area of 0.4 $m^2$ with different tilt angles, and the second method is a greenhouse effect in the solar dryer itself. They found that the first method took 24 h to decrease the moisture content from 60% to 10% at 45°C, whereas the drying time was reduced to 10 h by using both methods. Arun et al. [3] studied the drying kinetics of unripe banana chips of thickness 2–4 mm with a diameter range of 40–45 mm in a multi-plate mixed-mode flat plate solar dryer combined with a short-term energy-storing device called a separate metallic cylinder, and they reported that the maximum solar collector outlet temperature was 63°C. Ezeanya et al. [4] studied and assessed the relationship among the distributed forced convection type flat-plate solar collector with a dull black painted mild steel flat absorber plate and 4 mm glass cover for the drying of Ogbono seeds. They observed that the maximum drying rate of 10.03%/h was obtained for the collector plate area of 0.60 $m^2$, the tilt angle of 5°, and the plate thickness of 2.70 mm. Kadam and Samuel [5] established and tested a four-forced convective solar flat-plate collector with a black painted GI ribbed absorber plate of area 2 $m^2$, and a 4 mm glass cover, insulated with 25 mm thick thermocol, in a series of dryings of pre-treated cauliflower in a single layer. They reported that the temperature increased from 1.71°C to 13.51°C. Amer et al. [6] developed, fabricated, and tested a hybrid flat-plate type solar dryer with a 2 mm-thick ribbed GI absorber plate, a 4 mm glass cover, and a collector area of about 5.04 $m^2$, equipped with three solar reflected mirrors, a heat exchanger, and a heat storage unit to dry about 30 kg of ripe banana cuts. They stated that during the drying period, the average collector air temperature was 54.31°C which is 27°C above the ambient temperature. Pangavhane et al. [7] evaluated the thermal kinetic and drying characteristics of a natural convection solar dryer consisting of a black-coated aluminium flat plate absorber with a 4 mm glass cover and glass wool as insulation for drying grapes. They reported that the drying period of the grapes was shortened by 43% compared with the open-sun drying. Abubakar et al. [8] developed, tested, and related the drying performance of the mixed mode flat plate solar dryer with a GI sheet absorber plate and 4 mm glass cover, with and without heat storage medium, for the drying of about 7.0 kg of yam pieces. They expressed that the drying rates were $2.82 \times 10^{-5}$ kg/s and $2.55 \times 10^{-5}$ kg/s and reported that the drying rate with the storage materials was enhanced by about 13%. El Khadraoui et al. [9] examined experimentally and mathematically the drying of red pepper of about 80 kg in a forced convection mixed method of solar greenhouse dryer containing a flat plate solar collector. The authors revealed that the temperature of the drying air inside the greenhouse was from 29.21°C to 49.88°C, and the temperature of the drying air at the outlet of the solar collector was from 27.87°C to 54.68°C.

Gulcimen et al. [10] investigated experimentally and analytically the drying factors of solar air dryers consisting of flat plate solar collectors for drying sweet basil with fins fitted at diverse angles like 30°, 45°, and 60°. They reported that the moisture ratios decreased rapidly to 300 min for 0.012 kg/s, 360 min for 0.026 kg/s, and 450 min for 0.033 kg/s, with respect to the solar radiation that ranged between 440 and 750 W/$m^2$. Mewa et al. [11] evaluated the drying performance of a solar tunnel dryer, partly with a forced convection flat plate solar dryer, for beef drying; they reported that the drying speed of the solar dryer was greater than open-sun drying. Abene et al. [12] studied and observed the performance of a forced convection flat plate solar dryer for drying grapes. They found that the collector-supplied air with hindrances improved more than that without hindrances. Slama and Combarnous [13] designed and established an indirect forced convection flat plate solar dryer for drying orange peels, with various types of baffles placed cross-wise and longitudinal-wise. They found that the moisture content on a wet basis was reduced from 76% to 13% in 1 d. Seshachalam et al. [14] developed and assessed the performance of a triple-pass indirect forced convection solar dryer with a flat plate solar collector area of about 2 $m^2$ combined with a packed bed (sand) and a wire mesh absorber flat plate for drying 5 mm-thick carrot pieces. The authors reported that the collector outlet air temperature was 12°C greater than the ambient temperature. Vijayan et al. [15] established and studied the exergy and environmental effect of the indirect forced convection solar air dryer consisting of a solar flat plate collector of about 2 $m^2$ area with a black painted corrugated GI absorber plate, combined with a porous pebble as sensible heat energy storage materials for drying 4 kg of bitter gourd pieces. They found that the mass of the bitter gourd slices was reduced from 4,000 g to 723 g in 7 h at the mass flow rate of air of 0.0636 kg/s in the solar drying system. Kalaiarasi et al. [16] designed and fabricated solar air collectors of two different types. In Type I, a flat plate solar air collector with a black-coated aluminium sheet of about 0.4 mm thickness and an absorber plate was used, and in Type II, the same solar collector combined with heat-storing materials like synthetic oil was used. The authors concluded that the established solar heater with sensible heat storage at the absorber plate improved the thermal output and therefore led to consistent performance. Bhardwaj et al. [17] investigated experimentally the drying kinetics of an indirect forced convection type solar air dryer with a flat plate integrated with diverse combinations of sensible heat storage mediums such as (i) gravel, (ii) sand, (iii) gravel with iron scrap, (iv) sand with iron scrap, and (v) engine oil in a copper tube. They reported that the drying period was reduced by 37.50% by using heat pump drying and by 64.29% by using open sun drying.

Azaizia et al. [18] designed, fabricated, and inspected the drying performance of a novel type of forced convection solar dryer with and without heat energy storage using phase change materials (PCM) of about 45 kg of paraffin wax for drying red pepper cuts. They stated that the time taken to reduce the moisture content with PCM was 30 h,

whereas it took 55 h without PCM and 75 h with the open sun drying. Aboul-Enein et al. [19] studied and estimated the thermal performance of flat-plate solar air heaters with and without thermal storage materials (granite, sand, and water) and considered the effects of design factors such as length (L) and width (W). They found that the distinctive values of length 3 m and width 2 m improved the dryer's performance. Vijayan et al. [20] examined experimentally as well as theoretically the thermal kinetics of the flat plate solar collector of an area of about 2 $m^2$, with a GI corrugated absorber flat plate of 0.45 mm thickness, with and without heat energy storage materials (porous pebble bed). They found that the solar collectors with the packed bed were capable of delivering hot air in the range of 45°C to 60°C for a longer period, which could be preferred for achieving a better quality of the dried products.

Sabahi et al. [21] designed, fabricated, and evaluated the performance of a multiple-lamp solar simulator using a steady-state collector made with six 2,000 W and six 1,000 W of metal halide lamps placed in a decussate manner for industrial purposes. Metal halide lamps are a source of radiation. Gallo et al. [22] investigated the various types of solar simulators using different lamps like metal halide lamps, xenon arc lamps, argon lamps, halogen lamps, etc., and they discussed the different applications of solar simulators with single-lamp and multiple-lamps and highlighted the benefits and disadvantages of the specific solar simulator. Tawfik et al. [23] studied the solar simulator to examine the performance of the lamp system and correlated it to a regular source of sunlight. They reviewed the obtainable light sources with high-flex and low-flex solar simulators using diverse types of lamps. The authors concluded that metal halide lamps and xenon arc lamps are superior to other lamps. Song et al. [24] developed and established a flexible solar simulator with a high-flex xenon lamp along with a multiple-component optical-fibre package in an ellipsoidal truncated mirror glass array with an essential concentrator and reported that solar simulators have mostly used metal halide lamps, xenon arc lamps, lasers, and organ lamps. Ekman et al. [25] studied high-flux solar simulators in their research and development processes. Sarwar et al. [26] investigated an indoor solar thermal simulator using 7 kW xenon arc lamps of high power, with the output of the highest flux of 3,583 kW/$m^2$, used for the performance evaluation of the solar thermal simulator.

Satter [27] studied using the Taguchi method to optimize the performance factors for dehydrating copra to a safe moisture content level of 6% with different types of dryers with respect to the fuel used. They studied three factors, *viz.*, copra particle size, air temperature, and air velocity. They presented that temperature had the maximum effect on copra drying, whereas factors such as particle size and air speed were not significant. Tasirin et al. [28] examined, using the Taguchi technique, optimizing the drying factors of orange skins in a fluidized bed dryer. The operating factors such as the velocity of air (0.67, 0.85, and 1.03 m/s), temperature (60°C and 70°C), and orange peel with sand mass mixing ratios of 1:0 and 1:10 were used in their study. The optimized results displayed by the authors are the drying velocity at 1.03 m/s, the temperature at 70°C, and the orange peel-to-sand mass mixing ratio at 1:10. Osodo [29] estimated and optimized the factors of the forced convective solar desiccator under laboratory and open-sun conditions. The factors used were grain layer thickness, the temperature of the air, and drying air velocity to study and raise the performance using Taguchi's method under diverse drying conditions.

The comprehensive analysis of the literature exhibits strong information. Even though numerous researchers have reported harvesting hot air with the assistance of a secondary medium, very few studies have described the use of flat plate solar air heaters (FPL-SAH) with diverse influencing factors for direct air heating procedures. Also, it is understood that appropriate guidance of air inside FPL-SAH is specifically needed to improve thermal performance. The air mass flow rates reported in the existing air through the sensible heat-storing medium and twin copper fin flat plate arrangement can increase thermal efficiency. It is apparent that the major disadvantage of solar dryers is that they function only during sunny times; hence, they cannot be used for drying applications after sunset. Some agricultural products need an extended period of time to dry continuously for several days. For crops that require non-stop continuous drying, an indoor lamp simulator is the best option for continuous and off-sunshine periods. In this research study, a halogen lamp setup is used as a source of heat, combined with the existing solar air heater. The experiments were conducted by applying Taguchi's technique with five factors at three levels that influence the temperature gain and finding the most significant factors and their order of importance, along with the interactions between them.

## 2. Materials and methods

### 2.1. Experimental setup

The FPL-SAH with two copper flat fins was designed, fabricated, and mounted inside the building. The experimental arrangement includes key components such as a solar collector, a halogen lamp, and a blower that is used to circulate ambient air inside the setup.

A FPL-SAH is a distinctive type of heat exchanger that includes an absorbent plate under the clear glass cover with a specified space. It absorbs the heat from the light source and transmits it to the working fluid that flows underneath the absorber plate. It transports the hot air at moderate temperatures up to 100°C. It is comparatively modest in construction and less expensive to fabricate, install, and maintain. In this work, a flat plate solar air heater of size 700 mm × 400 mm × 180 mm was used. The bottom plate and the sides of the solar heater box were made of a galvanized iron sheet (GI) 1 mm thick. A black-painted, 0.8-mm-thick copper flat-plate was used as an absorber plate material, and the equipment was designed in such a way that other absorber plate materials, *viz.*, galvanized iron or aluminium sheet, could be easily assembled or disassembled for a comparison study on their performance. The holes provided on the absorber plate for joining purposes were wrapped with an airtight washer made of polystyrene foam to avoid leakage. All four sides of the solar heater box were insulated using thermocol of 25 mm thickness and 50 mm on the bottom side of the heater box. (Other insulating materials, *viz.*, coconut fibre and glass wool, were also used in this research

study.) The top side of the solar heater box was covered using plain transparent glass of 4 mm thickness (the glass covers of 5 and 6 mm thickness were also used for the performance study). A gap of 30 mm was maintained between the absorber plate and the glass cover to diminish the convective heat loss to the surroundings. The detailed cross-sectional view of FPL-SAH is shown in Fig. 1. The technical specification of the air simulator is shown in Table 1.

The four top corners of the heater box were sealed with airtight tape after fixing the glass cover to get the desired air mass flow rate without a leak. To effectively transfer the heat from the absorbing plate to the air medium, two additional distinctive types of copper fin flat plates of size 0.8 mm thick, 60 mm wide at the top side, and 30 mm wide at the bottom side were used, which also served as an additional support to the absorber flat plate at the top side (60 mm side of the fins) and were fastened using screws, nuts, and washers, as shown in Fig. 2.

These fins are the most effective arrangement to extract the maximum amount of radiance light falling on the absorber plate and transfer it to copper scrap, introduced as sensible heat-storing materials (the other types of sensible heat-storing materials are iron scraps or aluminium scraps used in this research) in the airflow passage between the absorber flat plate and the bottom plate of the solar collector box. Copper scrap was filled to a height of 80 mm in all

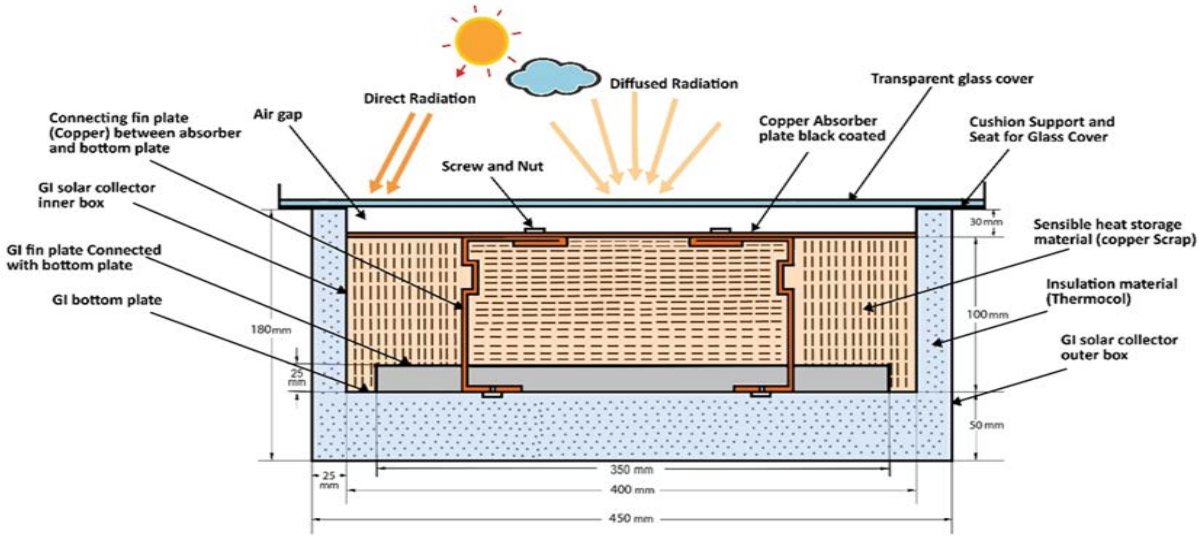


Fig. 1. Cross-sectional view of the solar air simulator box (Selvaraj et al. [30]).

Table 1
Technical specifications of the solar air simulator box

| S. No. | Description | Specification |
|---|---|---|
| 1 | Type of solar air heater | Flat absorber plate, active type |
| 2 | Aperture area of the heater ($A_{ap}$) | 0.28 m$^2$ |
| 3 | Dimensions of the absorber flat plate | 0.7 m × 0.4 m |
| 4 | Absorber plate material | 0.8 mm thick copper plate (aluminium or GI) |
| 5 | Type of absorber plate | Flat-type plate |
| 6 | Absorber painting | Black coated |
| 7 | Number of glass covers | Single |
| 8 | Top glass cover material | Window glass, 4 mm thick (5 or 6 mm) |
| 9 | Spacing between glass and absorber | 30 mm |
| 11 | Mode of air mass flow | Forced convection type |
| 12 | Number of air passes | Single-pass |
| 13 | Air channel height | 100 mm |
| 14 | Back insulation for the heater | Coconut fiber (thermocol or glass wool) |
| 15 | Side insulation for the heater | Coconut fiber (thermocol or glass wool) |
| 16 | Blower specifications | Single phase 0.320 kW, centrifugal type |
| 17 | Air mass flow rate | 0.02 kg/s (0.03 or 0.04 kg/s) |
| 18 | Sensible heat-storing materials | Copper scrap (aluminium or iron scrap) |

three sections of the heater box to act as a sensible heat-storing medium, as shown in Fig. 3. The heat storage material provides reliable hot air for drying purposes. The entire arrangement was fabricated using 1 mm of GI sheet. The total experimental system with solar air heater, halogen lamp setup, and blower with data logger was organized as shown in Fig. 4. Rubber beading, duct tape, and polystyrene foam were used on all the fittings to minimize air leakage. To achieve a better air mass flow rate at the entrance of the air heater, a diverging portion (a rectangular duct

Fig. 2. Solar simulator is assembled with copper twin flat plates (Selvaraj et al. [30]).

Fig. 3. Solar simulator box is filled with copper scraps at the bottom (Selvaraj et al. [30]).

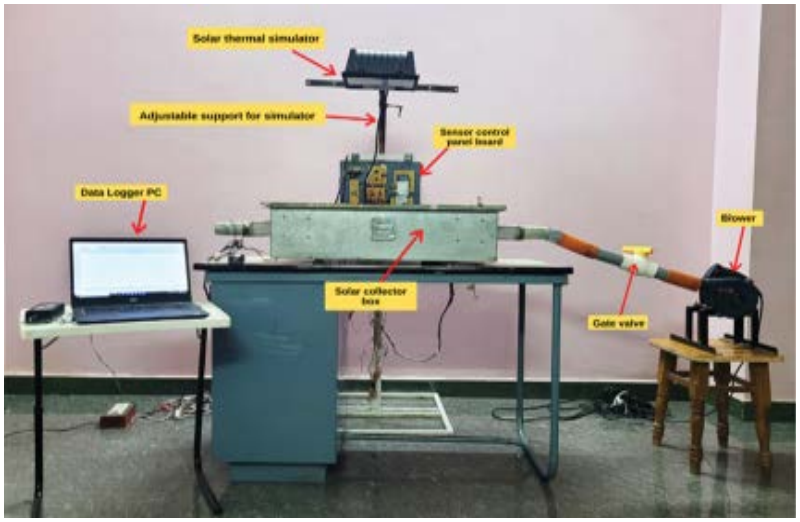


Fig. 4. Experimental setup with halogen lamp and sensors (Selvaraj et al. [30]).

of 125 mm × 45 mm connected to a 50 mm diameter circular duct) is attached to the solar simulator and the blower. Similarly, to confirm the better hot air mass flow rate from the heater to the drying unit, a converging duct portion was provided. A 320-Watt blower was connected by a flexible hose to supply the ambient air to the solar heater through a ball valve to vary the air mass flow rate.

### 2.2. Halogen lamp arrangement

The flat plate solar air simulator box is used in this experiment with a single 1,000-watt halogen lamp setup to supply heat energy is shown in Fig. 4 and the lamp specification is provided in Table 2.

### 2.3. Instrumentation

Before starting the experiment, the system was systematically checked for leaks. The established FPL-SAH was assisted with the essential measuring instruments to record the key factors of the system. To measure the temperatures of airflow passing through the heater, calibrated K-type thermocouples were positioned at appropriate points on the simulator, and they were linked to a data logger to record the temperature values at 10-min intervals. The recorded values can be brought into the computer system for further estimations. A vane-type anemometer, model HTC AVM-06 (ranged from 0–45 m/s with an accuracy of 3% of the velocity and ±0.5°C on temperature), is employed for the measurement of the velocity of air at the inlet and outlet of the solar simulator box for the estimation of air flow rate. The radiation of the lamp is recorded with the help of a solar meter (TES-1333 Instrument, Taiwan) with a range of 0 and 2,000 W/m$^2$, a resolution of 1 W/m$^2$, and an accuracy of ±10 W/m$^2$. The specifications of the instruments used in the present experiment are listed in Table 3.

Table 2
Specification of Crompton R7s halogen lamp: 1,000 W

| S. No. | Description | Values |
|---|---|---|
| 1 | Light item | Halogen lamp |
| 2 | Brand | Crompton R7s |
| 3 | Base type | R7s |
| 4 | Power | 1,000 W |
| 5 | Voltage | 240 V |
| 6 | Luminous flex | 20,000 Lumen |
| 7 | Diameter of the lamp | 10 mm |
| 8 | Length of the lamp | 189.1 mm |
| 9 | Shape | Tubular |
| 10 | Average life | 2,000 burning hours |
| 11 | Colour | Yellow |
| 12 | Frequency | 50 Hz |

### 2.4. Valuation of uncertainty

Experimental uncertainty valuation is of added importance as it determines the possible fault values in the measured and estimated readings since the faults in the experimental observations are unavoidable. In this experimental examination, the measured variables are the temperature of the air, lamp insolation, air mass flow rate, and relative humidity, and the calculated factors like useful heat gain, thermal efficiencies, and effective efficiencies are listed in Table 4. The uncertainty was assessed using Eq. (1), as suggested by Holman [31].

$$w_R = \left[\left(\frac{\partial R}{\partial x_1} w_1\right)^2 + \left(\frac{\partial R}{\partial x_2} w_2\right)^2 + \cdots + \left(\frac{\partial R}{\partial x_n} w_n\right)^2\right]^{1/2} \quad (1)$$

where $w_R$ is the uncertainty in the dependent or estimated variable, and $w_1$, $w_2$, …, $w_n$ are the uncertainties in the independent or measured variables.

## 3. Experimental methods

The performance evaluation of the flat plate solar air simulator was carried out with a diverse combination of five factors and their three levels, as shown in Table 5.

### 3.1. Experimental process

The thermal performance was conducted using the factors and their levels, which are shown in Table 5.

Table 4
Uncertainty values

| S. No. | Factors | Uncertainty |
|---|---|---|
| 1 | Temperature (°C) | ±0.304 |
| 2 | Air velocity (m/s) | ±0.17 |
| 3 | Lamp irradiance (W/m$^2$) | ±0.14 |
| 4 | Heat gain (Watts) | ±0.4623 |

Table 3
Specification of instruments

| Name of the instrument | Purpose | Make/Model | Range | Resolution | Accuracy |
|---|---|---|---|---|---|
| Solar meter | To measure the lamp irradiance | TES-1333 | 2,000 W/m$^2$ | 1 W/m$^2$ | ±10 W/m$^2$ |
| Vane-type anemometer | To measure the velocity of airflow entering and leaving the simulator | HTC AVM-06 | 0°C–50°C<br>0–45 m/s | 0.1°C<br>0.01 m/s | ±0.5°C<br>on 0°C–45°C<br>±3% on velocity |
| Thermocouple | To measure the temperature at various points | *k*-type | 0°C–450°C | 0.1°C | ±0.5°C |

Table 5
Taguchi design of experiments using the L27 orthogonal array (five factors and its three levels)

| Ex. No. | Insulator material | Glass cover thickness (mm) | Absorber flat plate material | Sensible heat-storing material | Air mass flow rate: kg/s ($\dot{m}$) |
|---|---|---|---|---|---|
| 1 | Thermocol | 4 | Copper | Copper scrap | 0.01 |
| 2 | Thermocol | 4 | Copper | Copper scrap | 0.02 |
| 3 | Thermocol | 4 | Copper | Copper scrap | 0.03 |
| 4 | Thermocol | 5 | Aluminium | Aluminum scrap | 0.01 |
| 5 | Thermocol | 5 | Aluminium | Aluminum scrap | 0.02 |
| 6 | Thermocol | 5 | Aluminium | Aluminum scrap | 0.03 |
| 7 | Thermocol | 6 | Galvanized iron | Iron scrap | 0.01 |
| 8 | Thermocol | 6 | Galvanized iron | Iron scrap | 0.02 |
| 9 | Thermocol | 6 | Galvanized iron | Iron scrap | 0.03 |
| 10 | Coconut fibre | 4 | Aluminium | Iron scrap | 0.01 |
| 11 | Coconut fibre | 4 | Aluminium | Iron scrap | 0.02 |
| 12 | Coconut fibre | 4 | Aluminium | Iron scrap | 0.03 |
| 13 | Coconut fibre | 5 | Galvanized iron | Copper scrap | 0.01 |
| 14 | Coconut fibre | 5 | Galvanized iron | Copper scrap | 0.02 |
| 15 | Coconut fibre | 5 | Galvanized iron | Copper scrap | 0.03 |
| 16 | Coconut fibre | 6 | Copper | Aluminum scrap | 0.01 |
| 17 | Coconut fibre | 6 | Copper | Aluminum scrap | 0.02 |
| 18 | Coconut fibre | 6 | Copper | Aluminum scrap | 0.03 |
| 19 | Glass wool | 4 | Galvanized iron | Aluminum scrap | 0.01 |
| 20 | Glass wool | 4 | Galvanized iron | Aluminum scrap | 0.02 |
| 21 | Glass wool | 4 | Galvanized iron | Aluminum scrap | 0.03 |
| 22 | Glass wool | 5 | Copper | Iron scrap | 0.01 |
| 23 | Glass wool | 5 | Copper | Iron scrap | 0.02 |
| 24 | Glass wool | 5 | Copper | Iron scrap | 0.03 |
| 25 | Glass wool | 6 | Aluminum | Copper scrap | 0.01 |
| 26 | Glass wool | 6 | Aluminum | Copper scrap | 0.02 |
| 27 | Glass wool | 6 | Aluminum | Copper scrap | 0.03 |

The experimental system was initially allowed to run for 30 min to reach the steady-state condition before taking the readings. After 30 min of the initial run, the room temperature (inlet temperature), humidity level, lamp radiation, humidity level at the outlet, air mass flow rate, and outlet temperature were measured and recorded. The experiments were repeated three times for the factors and their levels as per the L27 orthogonal array.

### *3.2. Performance investigation of the solar simulator*

The thermal performance of the solar air simulator is usually communicated with the important performance indicators of the major apparatuses of the system, such as the outlet air temperature and the useful heat gain of the solar air simulator. Since the total number of 27 experiments is greater and is repeated three times for averaging out of the variable errors, only the data of five samples of experiments, *viz*. 3, 8, 16, 20, and 23, are presented in Tables 6–10, respectively.

The average temperature gains of all 27 experiments were plotted as shown in Fig. 5. It indicates the variation of the mean solar simulator temperature gain concerning the matching of the experiment numbers. Experiment number 16 shows that there is a maximum temperature gain of 16.35°C. The plots also indicate variations in all the experiments, and they may be due to the atmospheric temperature and humidity level changes from morning to night inside the room, and further voltage fluctuations during the experimentation may also contribute to the variations.

## 4. Results and discussions

The experiments conducted were analysed for the signal-to-noise ratio "the greater the better". The analysis results are shown in Table 11, and the main effect plot for signal-to-noise ratio and the mean of means are plotted and are shown in Figs. 6 and 7, respectively. The analysis report specifies that the most significant factor in this experimental setup is the insulation, followed by a heat-absorbing plate. The other factors, like air mass flow, sensible heat-storing material, and the top glass cover, have a significant level in the declining order, as shown in Table 11.

From the main effect plots for the S/N ratio shown in Fig. 6 and the means shown in Fig. 7, it is perceived that the insulation done by coconut fibre has given greater thermal

Table 6
Experimental data obtained in experiment no. 3

| Ex. No. | Insulating material | Glass cover thickness | Absorber flat plate material | Sensible heat-storing material | Air mass flow rate ($\dot{m}$) | Outlet temp. (°C) ($T_{fo}$) | Temperature gain (°C) |
|---|---|---|---|---|---|---|---|
| 3 | Thermocol | 4 mm | Copper | Copper scrap | 0.03 kg/s | | |
| Time | Room temperature (°C) | Room RH (%) | Lamp radiation ($I_t$) (W/m$^2$) | Outlet RH (%) | Inlet temperature (°C) ($T_{fi}$) | | |
| 7.00 PM | 36.5 | 52.2 | 220.56 | 32 | 35.35 | 44.2 | 8.85 |
| 7.10 PM | 36.5 | 52.1 | 223.2 | 31.5 | 35.75 | 44.3 | 8.55 |
| 7.20 PM | 36 | 51 | 224.8 | 30.2 | 35.75 | 45.2 | 9.45 |
| 7.30 PM | 36 | 50.5 | 226.4 | 28.5 | 35.6 | 47.2 | 11.6 |
| Average | 36.17 | 51.20 | 224.80 | 30.07 | 35.70 | 45.57 | 9.87 |

Table 7
Experimental data obtained in experiment no. 8

| Ex. No. | Insulating material | Glass cover thickness | Absorber flat plate material | Sensible heat-storing material | Air mass flow rate ($\dot{m}$) | Outlet temp. °C ($T_{fo}$) | Temperature gain (°C) |
|---|---|---|---|---|---|---|---|
| 8 | Thermocol | 4 mm | Copper | Copper scrap | 0.02 kg/s | | |
| Time | Room temperature (°C) | Room RH (%) | Lamp radiation ($I_t$) (W/m$^2$) | Outlet RH (%) | Inlet temperature (°C) ($T_{fi}$) | | |
| 11.00 AM | 31 | 60.7 | 207.04 | 37.7 | 31.1 | 42 | 10.9 |
| 11.10 AM | 31 | 57.2 | 207.12 | 36.5 | 32 | 43 | 11 |
| 11.20 AM | 31.5 | 55 | 212.4 | 34.2 | 32.35 | 43.7 | 11.35 |
| 11.30 AM | 32 | 51 | 206.24 | 33 | 33.25 | 44.2 | 10.95 |
| Average | 31.50 | 54.40 | 208.59 | 34.57 | 32.53 | 43.63 | 11.10 |

Table 8
Experimental data obtained in experiment no. 16

| Ex. No. | Insulating material | Glass cover thickness | Absorber flat plate material | Sensible heat-storing material | Air mass flow rate ($\dot{m}$) | Outlet temp. °C ($T_{fo}$) | Temperature gain in °C |
|---|---|---|---|---|---|---|---|
| 16 | Coconut fibre | 6 mm | Copper | Aluminium scrap | 0.01 kg/s | | |
| Time | Room temperature (°C) | Room RH (%) | Lamp radiation ($I_t$) (W/m$^2$) | Outlet RH (%) | Inlet temperature (°C) ($T_{fi}$) | | |
| 2.50 PM | 37 | 49 | 214.96 | 26 | 37 | 50.2 | 13.2 |
| 3.07 PM | 37 | 44.2 | 212 | 21 | 37.1 | 52.7 | 15.6 |
| 3.17 PM | 37 | 43 | 237.6 | 20.8 | 37.35 | 54.2 | 16.85 |
| 3.28 PM | 37 | 39.5 | 234.64 | 20.2 | 37.5 | 54.1 | 16.6 |
| Average | 37.00 | 39.5 | 228.08 | 20.2 | 37 | 50.2 | 16.35 |

gain, followed by thermocol, and glass wool provided the least output. This may be acceptable based on the effective thermal resistance of the coconut fibre amongst all insulating materials used in this experiment, as shown in Fig. 8. The effective thermal resistance plot shown in Fig. 8 is based on the estimation carried out using the insulating materials' properties, *viz.* thermal conductivity and density as shown in Table 12.

The 2nd plot in Figs. 6 and 7 displays that the greater temperature gain is attained in the case of a 4 mm top glass cover. This is owing to more heat transmission across the smaller glass thickness out of the three levels used in these experiments satisfying the basic thermal conductance equation. The greater the thickness, the smaller the amount of heat transferred across the glass.

The 3rd plot shown in Figs. 6 and 7 indicates that the copper absorber flat plate has a greater gain in output temperature owing to its higher thermal conductivity and henceforth transfers more thermal energy to the storing medium, thereby producing better performance in contrast

Table 9
Experimental data obtained in experiment no. 20

| Ex. No. | Insulating material | Glass cover thickness | Absorber flat plate material | Sensible heat-storing material | Air mass flow rate ($\dot{m}$) | Outlet temp. °C ($T_{fo}$) | Temperature gain °C |
|---|---|---|---|---|---|---|---|
| 20 | Glass wool | 4 mm | GI sheet | Aluminium scrap | 0.02 kg/s | | |
| Time | Room temperature (°C) | Room RH (%) | Lamp Radiation ($I_t$) (W/m$^2$) | Outlet RH (%) | Inlet temperature (°C) ($T_{fi}$) | | |
| 7.05 PM | 31 | 59.2 | 252.8 | 51.5 | 30.85 | 34.5 | 3.65 |
| 7.15 PM | 32 | 56.2 | 250.64 | 42.5 | 32 | 38.2 | 6.2 |
| 7.25 PM | 32 | 55 | 248 | 37.2 | 32 | 41 | 9 |
| 7.35 PM | 32 | 52.5 | 251.36 | 32.7 | 32.35 | 43.7 | 11.35 |
| Average | 32.00 | 52.5 | 250.00 | 32.7 | 30.85 | 34.5 | 8.85 |

Table 10
Experimental data obtained in experiment no. 23

| Ex. No. | Insulating material | Glass cover thickness | Absorber flat plate material | Sensible heat-storing material | Air mass flow rate ($\dot{m}$) | Outlet temp. (°C) ($T_{fo}$) | Temperature gain (°C) |
|---|---|---|---|---|---|---|---|
| 23 | Glass wool | 5 mm | Copper | Iron scrap | 0.02 kg/s | | |
| Time | Room temperature (°C) | Room RH (%) | Lamp radiation (W/m$^2$) | Outlet RH (%) | Inlet temperature (°C) ($T_{fi}$) | | |
| 2.00PM | 32 | 56.5 | 231 | 38.5 | 32.1 | 41.7 | 9.6 |
| 2.10 PM | 32.8 | 54.2 | 238 | 33.7 | 33.4 | 45.2 | 11.8 |
| 2.20 PM | 33 | 50 | 241 | 31.1 | 34.35 | 47 | 12.65 |
| 2.30 PM | 33.9 | 49.7 | 245 | 29.7 | 34.8 | 48.2 | 13.4 |
| Average | 33.23 | 49.7 | 241 | 29.7 | 32.1 | 41.7 | 12.62 |

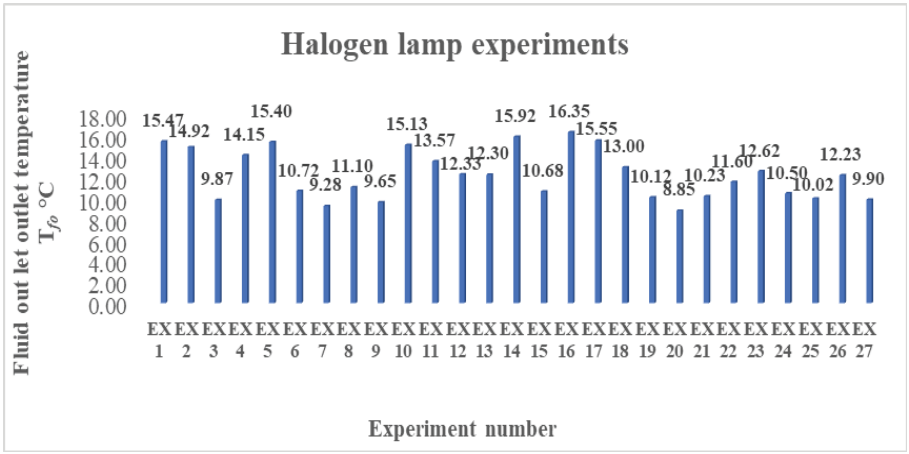


Fig. 5. Simulator outlet average temperature gain vs. experiment numbers.

with the aluminium and galvanized iron sheets of the same sizes.

From the 4th plot shown in Figs. 6 and 7, it is observed that the aluminium scraps used as a storage material have improved performance due to their effective storing of heat due to their lower density, high specific heat, and higher surface area in comparison with the copper scraps and iron scraps, and hence they are capable of delivering heat energy at higher temperatures.

Lastly, in the 5th plot, as shown in Figs. 6 and 7, it is detected that the air mass flow rate of 0.02 kg/s has improved temperature gain in contrast to the mass flow rates of air at 0.01 and 0.03 kg/s. At a lower air mass flow rate from the blower to the heating simulator, the airflow mass may be

Table 11
Response for signal-to-noise ratios
The larger, the better

| Level | Insulation | Glass cover | Absorb plate | Sensible Mtl. | Air mass flow (kg/s) ($\dot{m}$) |
|---|---|---|---|---|---|
| 1 | 23.20 | 22.17 | 22.09 | 22.27 | 22.33 |
| 2 | 20.71 | 22.01 | 22.72 | 21.93 | 22.59 |
| 3 | 21.90 | 21.63 | 20.99 | 21.60 | 20.88 |
| Delta | 2.48 | 0.54 | 1.73 | 0.66 | 1.71 |
| Rank | 1 | 5 | 2 | 4 | 3 |

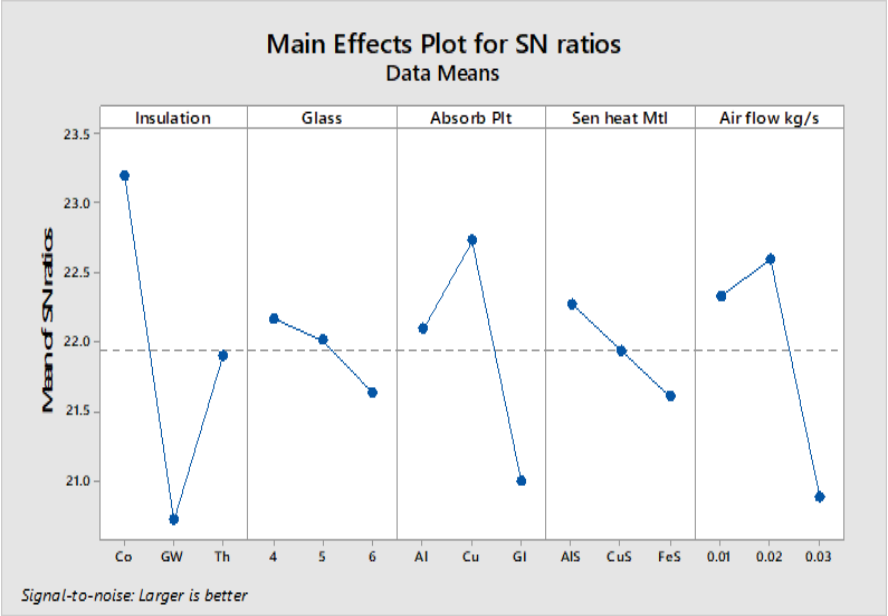


Fig. 6. Main effect plots for signal-to-noise ratios.


Fig. 7. Main effect plots for means.

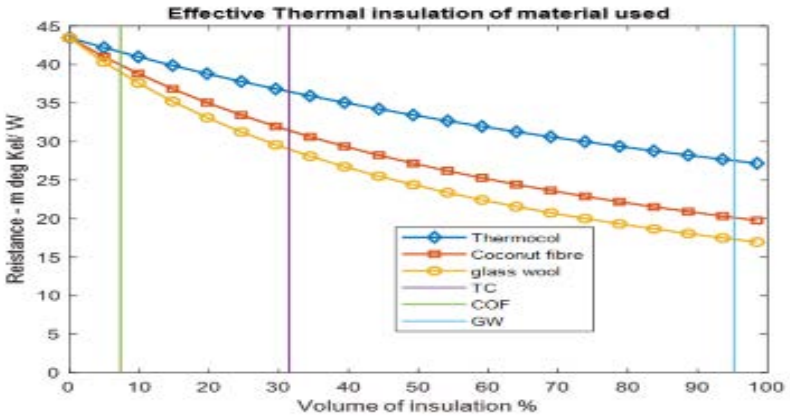


Fig. 8. Effective thermal insulation due to the existence of air in the simulator.

Table 12
Insulating material properties and effective conductance

| S. No. | Insulating medium | Density (kg/m$^3$) | Thermal conductivity (K) (W/m·°C) | Mass of insulating material (kg) | Effective conductivity area (m$^2$) | Total conductance = (conductance of insulating material + conductance of air) × effective area | Effective heat-resistance (°C/W) |
|---|---|---|---|---|---|---|---|
| 1 | Thermocol | 15–30 | 0.029–0.045 | 0.144 | 31 | 0.02734 | 36.57 |
| 2 | Coconut fiber | 785–1,150 | 0.043–0.06 | 1.432 | 7.3 | 0.025 | 40 |
| 3 | Glass wool | 20–100 | 0.039–0.08 | 1.45 | 95 | 0.052 | 19.2 |

Table 13
Response table for means

| Level | Insulation material | Glass cover | Absorb plate | Sensible heat Mtl. | Air mass flow (kg/s) ($\dot{m}$) |
|---|---|---|---|---|---|
| 1 | 14.63 | 13.04 | 12.93 | 13.28 | 13.40 |
| 2 | 10.89 | 12.73 | 13.89 | 12.67 | 13.61 |
| 3 | 12.64 | 12.38 | 11.33 | 12.21 | 11.14 |
| Delta | 3.73 | 0.66 | 2.56 | 1.07 | 2.47 |
| Rank | 1 | 5 | 2 | 4 | 3 |

Table 14
Optimum parameter combination

| S. No. | Control factor | Parameter | Level |
|---|---|---|---|
| 1 | Insulating material | Coconut fibre | 1 |
| 2 | Top glass cover thickness | 4 mm | 1 |
| 3 | Absorb flat plate material | Copper (sheet 0.8 mm thick) | 2 |
| 5 | Air mass flow rate ($\dot{m}$) | 0.02 kg/s | 2 |
| 6 | Sensible heat-storing material | 1 kg aluminium scrap | 2 |

inadequate to absorb energy inside the simulator, thereby dropping the flow of energy from the radiation source to the outlet, causing a lesser output temperature, while at a 0.03 kg/s air mass flow rate, the heat absorbed by the air is less due to less contact time, causing a low-temperature gain in the output. At 0.02 kg/s, the heat transmission rate is optimal, thereby achieving a better output temperature. Table 13 specifies the ranking of the factors in order of importance based on the delta value.

Based on the analysis of the L27 experiments carried out, the optimum factors of the above experiments are provided in Table 14.

The output after analysis of variance (ANOVA) for temperature improvement is shown in Table 15. It is found that the insulation and air mass flow rates, followed by absorbing resources, are the most important factors that contribute towards the temperature gain for drying applications, as the *P*-value is lower than 0.05 and the resultant *F*-values are

Table 15
General linear models: temperature gain vs. five factors chosen

| Factor coding | (–1, 0, +1) |
|---|---|

***Factor information***

| Factor | Type | Level | Value |
|---|---|---|---|
| Insulation material | Fixed | 3 | Co, GW, Th |
| Glass cover (mm) | Fixed | 3 | 4, 5, and 6 |
| Absorb plate | Fixed | 3 | Al, Cu, and GI |
| Sen heat material | Fixed | 3 | Al, Cu, and Fe scraps |
| Air mass flow (kg/s) ($\dot{m}$) | Fixed | 3 | 0.01, 0.02, and 0.03 |

***Analysis of variance***

| Source | DF | Adj. SS | Adj. MS | *F*-value | *P*-value |
|---|---|---|---|---|---|
| Insulation | 2 | 62.815 | 31.4076 | 16.53 | 0.000 |
| Glass cover | 2 | 1.992 | 0.9958 | 0.52 | 0.602 |
| Absorb plate | 2 | 30.083 | 15.0414 | 7.92 | 0.004 |
| Sen heat material | 2 | 5.190 | 2.5951 | 1.37 | 0.283 |
| Air mass flow kg/s ($\dot{m}$) | 2 | 33.748 | 16.8738 | 8.88 | 0.003 |
| Error | 16 | 30.400 | 1.9000 | | |
| Total | 26 | 164.227 | | | |

***Model summary***

| *S* | *R*-sq. | *R*-sq. (adjusted) | *R*-sq. (predicted) |
|---|---|---|---|
| 1.37839 | 81.49% | 69.92% | 47.29% |

***Coefficients***

| Terms | Co-ef. | SE Co-ef. | *T*-values | *P*-values | VIF |
|---|---|---|---|---|---|
| Constant | 12.719 | 0.265 | 47.95 | 0.000 | |
| | | Insulation | | | |
| Coconut | 1.909 | 0.375 | 5.09 | 0.000 | 1.33 |
| Glass wool | –1.825 | 0.375 | –4.86 | 0.000 | 1.33 |
| | | Glass cover | | | |
| 4 mm | 0.325 | 0.375 | 0.87 | 0.399 | 1.33 |
| 5 mm | 0.014 | 0.375 | 0.04 | 0.970 | 1.33 |
| | | Absorber plate | | | |
| Aluminium | 0.212 | 0.375 | 0.57 | 0.579 | 1.33 |
| Copper | 1.173 | 0.375 | 3.13 | 0.006 | 1.33 |
| | | Sen heat material | | | |
| Al scrap | 0.560 | 0.375 | 1.49 | 0.155 | 1.33 |
| Cu scrap | –0.051 | 0.375 | –0.13 | 0.894 | 1.33 |
| Air mass flow rate (kg/s) | ($\dot{m}$) | | | | |
| 0.01 | 0.685 | 0.375 | 1.82 | 0.087 | 1.33 |
| 0.02 | 0.892 | 0.375 | 2.38 | 0.030 | 1.33 |

larger. The $R^2$ value is 0.815 and fulfils the recommended value of >0.8 in a multiple linear regression investigation, and the data points are nearer to the fitted regression line.

From the examination of the experimental results, a regression equation is arrived at, as shown in Eq. (2). The equation can be utilized to predict and estimate the various levels of the influencing factors on the outlet temperature gain.

### 4.1. Regression line equation

$$\begin{aligned}\text{Temperature gain} = {} & 12.719 + 1.909\,\text{Insulation\_Co} - 1.825\,\text{Insulation\_GW} - 0.084\,\text{Insulation\_Thermocol} \\ & + 0.325\,\text{Glass\_4 mm} + 0.014\,\text{Glass\_5 mm} - 0.340\,\text{Glass\_6 mm} + 0.212\,\text{Absorb Plt\_Aluminium} \\ & + 1.173\,\text{Absorb Plt\_Copper} - 1.386\,\text{Absorb Plt\_GI} + 0.560\,\text{Sen heat material\_AlS(Al)} \\ & - 0.051\,\text{Sen heat material\_CuS(Cu)} - 0.510\,\text{Sen heat mtl\_FeS(Fe)} + 0.685\,\text{Air mass flow rate kg/s\_0.01} \\ & + 0.892\,\text{Air mass flow rate kg/s\_0.02} - 1.577\,\text{Air flow rate kg/s\_0.03}\end{aligned} \quad (2)$$

The residual chart for temperature gain is shown in Fig. 9. From the normal probability chart, it is observed that the maximum of the points is gathered around the straight line with a rising slope, indicating that the errors are roughly normal and follow the linear configuration. Considering the residual vs. fits, it is detected that half the points are above and half the points are below the zero line, and the scattering is random. The histogram designates a small deviation from normality, but since the sample is small, it need not be considered. Residual fits vs. the observation order specifies that the residuals are random and the variation is independent.

The predicted value based on the Taguchi technique is shown in Table 16, with an average temperature gain of 17.5790°C for coconut fibre, with 4 mm top glass, a copper absorber flat plate, and aluminium scrap with an air mass flow of 0.02 kg/s. In order to confirm the predicted values, three sets of experiments were carried out, and it was found that they deviated by less than 5%.

The interactive chart is shown in Fig. 10. It is observed that there is a strong interaction between the glass cover and absorber flat plate, the glass cover and insulation material, and the glass cover and sensible heat-storing medium. Additionally, it is noted that there is a weak interaction between air mass flow and storing medium, absorbing flat plate, glass cover, and insulation materials.

Based on the ANOVA analysis, the optimization was tested and visualized, as shown in Fig. 11. From the chart, the predictive factors for temperature gain were found to be for the coconut fibre, 4 mm glass cover, copper absorber

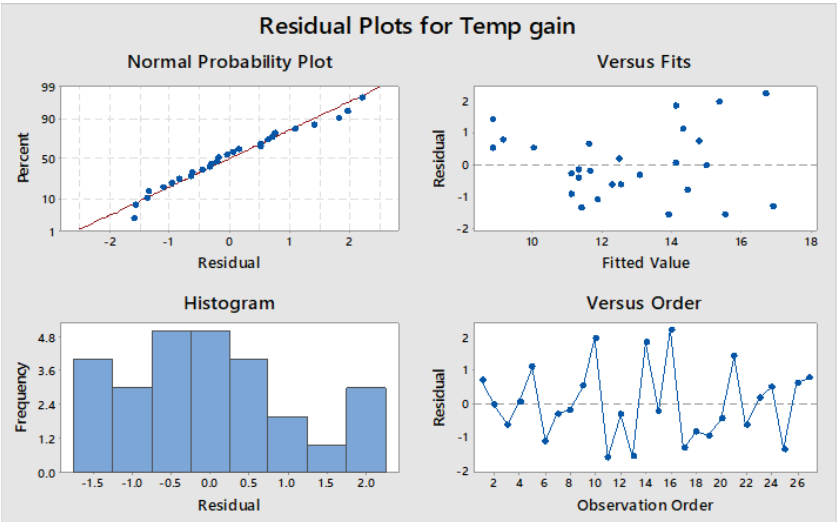


Fig. 9. Residual plots for temperature gain.

Table 16
Predicted values

| S/N ratio | | | Mean | |
|---|---|---|---|---|
| 25.2091 | | | 17.5790 | |
| Settings Insulation materials | Glass cover | Absorb plate material | Sensible heat-material | Air mass flow rate (kg/s) |
| Coconut fibre | 4 mm | Copper | Al-scrap | 0.02 |

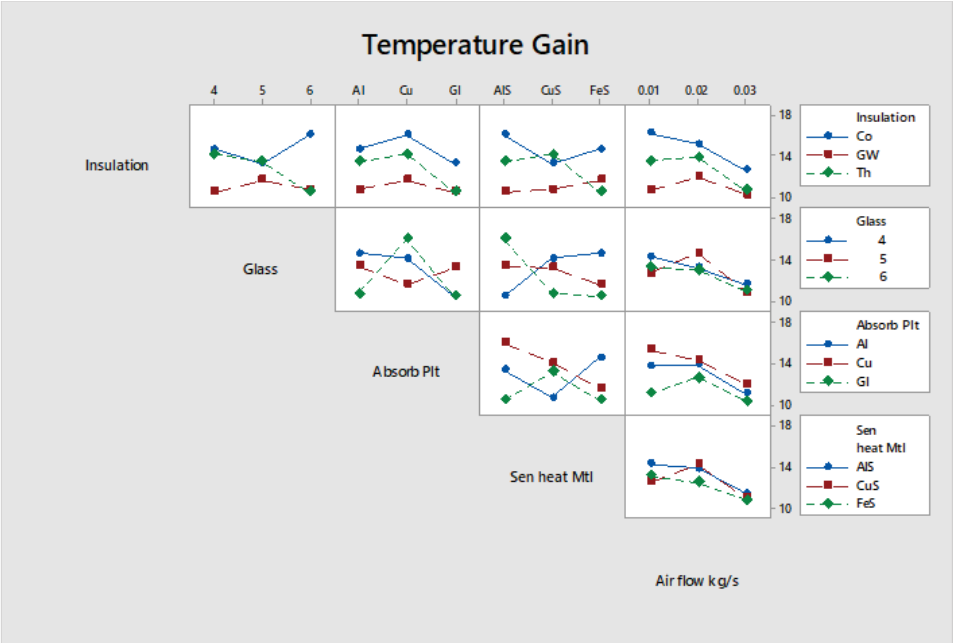


Fig. 10. Interaction plots.

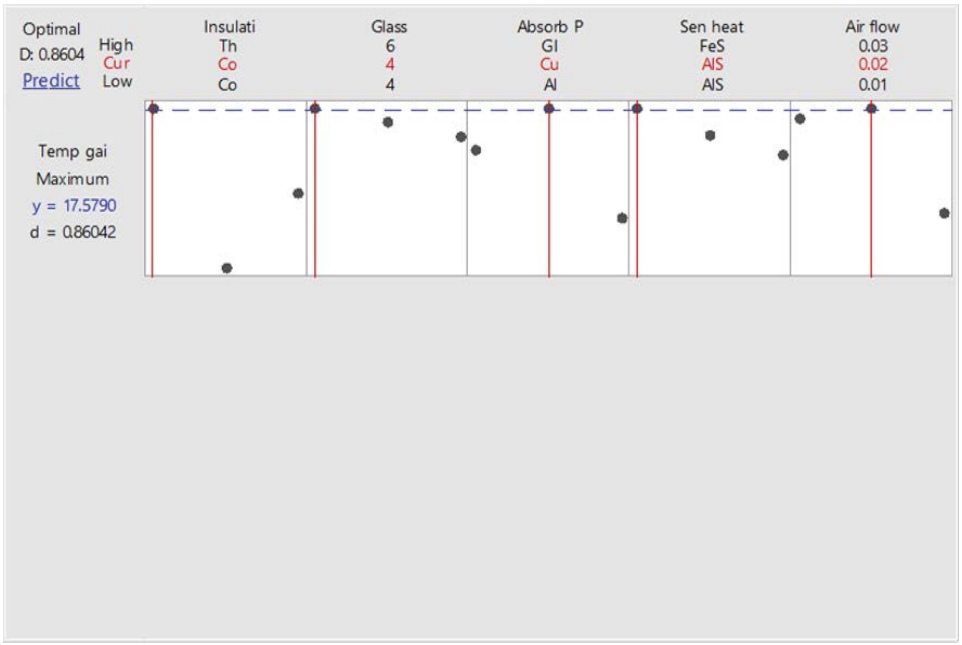


Fig. 11. Optimization plots.

flat plate, aluminium scrap as a storing medium with a forced air transmission of 0.02 kg/s. It is observed that the enhanced temperature gain was found to be 17.5790°C.

To confirm the expected values achieved by optimization, three sets of experiments were carried out with the parameters stated in the optimal outcome, and the values are documented as shown in Tables 17–19.

The validation results are consolidated in Table 20, and it is found that the validated test results are closely in agreement with the optimized value, and the inaccuracy percentage for the forecasted value is 2.37%, as shown in Table 20.

## 5. Conclusions

The indoor solar simulator with the solar collector box was used to study the five influencing factors and their three levels. Experiments were conducted using the Taguchi

Table 17
Estimated values of temperature gain in validity Test-1

| Second set of experiments | Insulating material | Glass cover thickness | Absorber plate material | Sensible storage material | Air mass flow rate ($\dot{m}$) | Outlet temp. (°C) ($T_{fo}$) | Temperature gain (°C) |
|---|---|---|---|---|---|---|---|
| Validity Test-1 | Coconut fibre | 4 mm | Copper metal | Aluminium scraps | 0.02 kg/s | | |
| Time | Room temperature (°C) | Room RH (%) | Lamp radiation ($I_t$) (W/m$^2$) | Outlet RH (%) | Inlet temperature (°C) ($T_{fi}$) | | |
| 3.30 PM | 32 | 68 | 213.6 | 32.7 | 32 | 49 | 17 |
| 3.40 PM | 32.2 | 64 | 212.08 | 31 | 32.2 | 50 | 17.8 |
| 3.50 PM | 33.2 | 62 | 212 | 31.2 | 33.2 | 50.2 | 17 |
| 4.00 PM | 32.7 | 62 | 200.88 | 31.2 | 32.7 | 50.2 | 17.5 |
| Average | 32.70 | 62 | 208.32 | 31 | 32 | 49 | 17.43 |

Table 18
Estimated values of temperature gain in validity Test-2

| Second set of experiments | Insulating material | Glass cover thickness | Absorber plate material | Sensible storage material | Air mass flow rate ($\dot{m}$) | Outlet temp. °C ($T_{fo}$) | Temperature gain (°C) |
|---|---|---|---|---|---|---|---|
| Validity Test-2 | Coconut fibre | 4 mm | Copper metal | Aluminium scraps | 0.02 kg/s | | |
| Time | Room temperature (°C) | Room RH (%) | Lamp radiation ($I_t$) (W/m$^2$) | Outlet RH (%) | Inlet temperature (°C) ($T_{fi}$) | | |
| 4.30 PM | 34 | 70 | 207.52 | 35.6 | 34 | 51.7 | 17.7 |
| 4.40 PM | 34 | 59.7 | 200.88 | 32.7 | 34 | 51.2 | 17.2 |
| 4.50 PM | 34.5 | 60 | 195.84 | 31 | 34.5 | 51 | 16.5 |
| 5.00 PM | 34 | 60 | 189.52 | 30.2 | 34 | 50.5 | 16.5 |
| Average | 34.17 | 59.90 | 195.41 | 31.30 | 34.17 | 50.90 | 16.73 |

Table 19
Estimated values of temperature gain in validity Test-3

| Second set of experiments | Insulating material | Glass cover thickness | Absorber plate material | Sensible storage material | Air mass flow rate ($\dot{m}$) | Outlet temp. °C ($T_{fo}$) | Temperature gain (°C) |
|---|---|---|---|---|---|---|---|
| Validity Test-3 | Coconut fibre | 4 mm | Copper metal | Aluminium scraps | 0.02 kg/s | | |
| Time | Room temperature (°C) | Room RH (%) | Lamp radiation ($I_t$) (W/m$^2$) | Outlet RH (%) | Inlet temperature (°C) ($T_{fi}$) | | |
| 5.30 PM | 32.5 | 71 | 2,123 | 31.1 | 32.5 | 50.2 | 17.7 |
| 5.40 PM | 32 | 67 | 2,050 | 31.7 | 32 | 49.5 | 17.5 |
| 5.50 PM | 32 | 57 | 2,195 | 32 | 32 | 49 | 17 |
| 6.00 PM | 31.2 | 65 | 2,138 | 32 | 31.2 | 48.7 | 17.5 |
| Average | 31.73 | 63.00 | 2,127.67 | 31.90 | 31.73 | 49.07 | 17.33 |

technique with an L27 orthogonal array using a 1,000-Watts single-halogen lamp as a source of light.

From the experimented results, it was found that most of the significant factors affecting the output temperature gain are in decreasing order: coconut fibre, copper absorber flat plate, air mass flow rate, aluminium sensible heat-storing material, and lastly, the top glass cover.

The enhanced output value of 17.579°C of temperature gain was estimated using ANOVA, and it was validated with the experimental results. The mean temperature gain of the three consecutive experiments was estimated at 17.16°C which is in close agreement with the predicted value, and the error was found to be only 2.37%.

## Symbols

FPL-SAH — Flat-plate solar air heater
$A_{ap}$ — Aperture area of the solar simulator box, m$^2$
$I_t$ — Lamp insolation falling on the simulator, W/m$^2$

Table 20
Validity check of the results of the three experiments

| Validity test No. | Insulator material | Glass cover thickness | Absorber plate material | Sensible heat-storage material | Air mass flow rate ($\dot{m}$) | Mean temperature gain |
|---|---|---|---|---|---|---|
| 1 | Coconut fibre | 4 mm | Copperplate | Aluminium scrap Aluminium | 0.02 kg/s | 17.43°C |
| 2 | Coconut fibre | 4 mm | Copperplate | Aluminium scrap | 0.02 kg/s | 16.73°C |
| 3 | Coconut fibre | 4 mm | Copperplate | Aluminium scrap | 0.02 kg/s | 17.3°C |
| Experimental average value | | | | | | 17.16°C |
| Based on the analysis of variance optimized value | | | | | | 17.58°C |
| Difference | | | | | | 0.42°C |
| Error percentage | | | | | | 2.37% |

$\dot{m}$ — Air mass flow rate, kg/s
$H$ — Air mass flow channel height, m
$T_{fi}$ — Fluid inlet temperature, °C
$T_{fo}$ — Fluid outlet temperature, °C
$R^2$ — Relationship between two variables
$L$ — Simulator length, m
$k$ — Thermal conductivity, W/m·K
PCM — Phase change material
GI — Galvanized iron sheet
Al — Aluminium
Cu — Copper
RH — Relative humidity
W — Watt
ANOVA — Analysis of variance
S/N — Signal-to-noise ratio
$F$-value — Value
$P$-value — Value
$w_1, w_2, \ldots, w_n$ — Uncertainties in the independent variables
$w_R$ — Uncertainty in the dependent variable

## References


[1] N.C. Ezeanya, C.C. Egwuonwu, A.B. Istifanus, V.C. Okafor, Determination of thin-layer solar drying kinetics of cassava noodles (tapioca), IJRET: Int. J. Res. Eng. Technol., 5 (2016) 352–360.
[2] H. Eustache, E. Dushimire, C. Amizero, Design and optimization of domestic solar dryer, Science, 5 (2017) 130–135.
[3] K.R. Arun, M. Srinivas, C.A. Saleel, S. Jayaraj, Active drying of unripened bananas (*Musa Nendra*) in a multi-tray mixed-mode solar cabinet dryer with backup energy storage, Sol. Energy, 188 (2019) 1002–1012.
[4] N.C. Ezeanya, K.N. Nwaigwe, P.E. Ugwuoke, Analysis of the effects of a flat plate solar dryer geometry on drying rate of agricultural seeds, Asian J. Agric. Sci., 4 (2012) 333–336.
[5] D.M. Kadam, D.V.K. Samuel, Convective flat-plate solar heat collector for cauliflower drying, Biosyst. Eng., 93 (2006) 189–198.
[6] B.M.A. Amer, M.A. Hossain, K. Gottschalk, Design and performance evaluation of a new hybrid solar dryer for banana, Energy Convers. Manage., 51 (2010) 813–820.
[7] D.R. Pangavhane, R.L. Sawhney, P.N. Sarsavadia, Design, development and performance testing of a new natural convection solar dryer, Energy, 27 (2002) 579–590.
[8] S. Abubakar, S. Umaru, M.U. Kaisan, U.A. Umar, B. Ashok, K. Nanthagopal, Development and performance comparison of mixed-mode solar crop dryers with and without thermal storage, Renewable Energy, 128 (2018) 285–298.
[9] A. El Khadraoui, I. Hamdi, S. Kooli, A. Guizani, Drying of red pepper slices in a solar greenhouse dryer and under open sun: experimental and mathematical investigations, Innovative Food Sci. Emerg. Technol., 52 (2019) 262–270.
[10] F. Gulcimen, H. Karakaya, A. Durmus, Drying of sweet basil with solar air collectors, Renewable Energy, 93 (2016) 77–86.
[11] E.A. Mewa, M.W. Okoth, C.N. Kunyanga, M.N. Rugiri, Experimental evaluation of beef drying kinetics in a solar tunnel dryer, Renewable Energy, 139 (2019) 235–241.
[12] A. Abene, V. Dubois, M. Le Ray, A. Ouagued, Study of a solar air flat plate collector: use of obstacles and application for the drying of grape, J. Food Eng., 65 (2004) 15–22.
[13] R.B. Slama, M. Combarnous, Study of orange peels dryings kinetics and development of a solar dryer by forced convection, Solar Energy, 85 (2011) 570–578.
[14] K. Seshachalam, V.A. Thottipalayam, V. Selvaraj, Drying of carrot slices in a triple pass solar dryer, Therm. Sci., 21 (2017) 389–398.
[15] S. Vijayan, T.V. Arjunan, A. Kumar, Exergo-environmental analysis of an indirect forced convection solar dryer for drying bitter gourd slices, Renewable Energy, 146 (2020) 2210–2223.
[16] G. Kalaiarasi, R. Velraj, M.N. Vanjeswaran, N.G. Pandian, Experimental analysis and comparison of flat plate solar air heater with and without integrated sensible heat storage, Renewable Energy, 150 (2020) 255–265.
[17] A.K. Bhardwaj, R. Chauhan, R. Kumar, M. Sethi, A. Rana, Experimental investigation of an indirect solar dryer integrated with phase change material for drying *Valeriana jatamansi* (medicinal herb), Case Stud. Therm. Eng., 10 (2017) 302–314.
[18] Z. Azaizia, S. Kooli, I. Hamdi, W. Elkhal, A.A. Guizani, Experimental study of a new mixed mode solar greenhouse drying system with and without thermal energy storage for pepper, Renewable Energy, 145 (2020) 1972–1984.
[19] S. Aboul-Enein, A.A. El-Sebaii, M.R.I. Ramadan, H.G. El-Gohary, Parametric study of a solar air heater with and without thermal storage for solar drying applications, Renewable Energy, 21 (2000) 505–522.
[20] S. Vijayan, T.V. Arjunan, A. Kumar, M.M. Matheswaran, Experimental and thermal performance investigations on sensible storage based solar air heater, J. Energy Storage, 31 (2020) 101620, doi: 10.1016/j.est.2020.101620.
[21] H. Sabahi, A.A. Tofigh, I.M. Kakhki, H. Bungypoor-Fard, Design, construction and performance test of an efficient large-scale solar simulator for investigation of solar thermal collectors, Sustainable Energy Technol. Assess., 15 (2016) 35–41.
[22] A. Gallo, A. Marzo, E. Fuentealba, E. Alonso, High flux solar simulators for concentrated solar thermal research: a review, Renewable Sustainable Energy Rev., 77 (2017) 1385–402.
[23] M. Tawfik, X. Tonnellier, C. Sansom, Light source selection for a solar simulator for thermal applications: a review, Renewable Sustainable Energy Rev., 90 (2018) 802–813.
[24] J. Song, J. Wang, Y. Niu, W. Wang, K. Tong, H. Yu, Y. Yang, Flexible high flux solar simulator based on optical fiber bundles, Sol. Energy, 193 (2019) 576–583.

[25] B.M. Ekman, G. Brooks, M.A. Rhamdhani, Development of high flux solar simulators for solar thermal research, Sol. Energy Mater. Sol. Cells, 141 (2015) 436–446.
[26] J. Sarwar, G. Georgakis, R. LaChance, N. Ozalp, Description and characterization of an adjustable flux solar simulator for solar thermal, thermochemical and photovoltaic applications, Sol. Energy, 100 (2014) 179–194.
[27] M.A. Satter, Design and Development of a Portable Copra Dryer, Proceedings of the International Conference on Mechanical Engineering 2003 (ICME2003) 26–28 December 2003, Dhaka, Bangladesh, 2003.
[28] S.M. Tasirin, I. Puspasari, L.J. Xing, Z. Yaakob, J.A. Ghani, Energy optimization of fluidized bed drying of orange peel using Taguchi method, World Appl. Sci. J., 26 (2013) 1602–1609.
[29] B.O. Osodo, Simulation and Optimization of a Drying Model for a Forced Convection Grain Dryer, Unpublished Ph.D. Thesis, Kenyatta University, Kenya, 2018.
[30] M. Selvaraj, P. Sadagopan, S. Vijayan, Investigation of thermal performance of an indirect forced convection solar dryer for tapioca chips drying, Desal. Water Treat., 230 (2021) 430–441.
[31] J.P. Holman, Experimental Methods for Engineers, McGraw-Hill Book Co., Singapore, 2011.